IEEE Access
Multidisciplinary | Rapid Review | Open Access Journal

Received September 24, 2019, accepted October 14, 2019, date of publication October 18, 2019, date of current version October 30, 2019.

Digital Object Identifier 10.1109/ACCESS.2019.2948210

VCT-AOC Comprehensive Method to Suppress High-Frequency Resonance and Low-Frequency Oscillation in Railway Traction Power Supply System

XINYU ZHANG, JIE CHEN, (Member, IEEE), RUICHANG QIU, AND ZHIGANG LIU
School of Electrical Engineering, Beijing Jiaotong University, Beijing 100044, China

Corresponding author: Jie Chen (jiechen@bjtu.edu.cn)

This work was supported by the Fundamental Research Funds for the Central Universities under Grant 2018JBM055.

ABSTRACT Aiming at the high-frequency resonance (HFR) and low-frequency oscillation (LFO) phenomena in high-speed railways, a comprehensive suppression method named voltage constant transient active oscillation compensation (VCT-AOC) is proposed. This method is optimized on the basis of AOC, and the adjustment time is shortened by the VCT suppression measure. When serious HFR happens, the system can be quickly restored and stabilized by completely removing the network voltage oscillation in the control part, thereby avoiding the transient overvoltage and overcurrent damage to the system. According to the characteristics of AOC and VCT, the VCT-AOC comprehensive suppression method is proposed, and the specific implementation scheme of this method is given. This paper established the train-network impedance model with AOC and VCT suppression methods. The Generalized Nyquist Analysis (GNA) method and the dominant pole analysis method are used to analyze the effect of VCT and AOC on the system. Finally, the effectiveness of suppression methods is verified by simulations and experiments.

INDEX TERMS Voltage constant transient active oscillation compensation, high-frequency resonance, low-frequency oscillation, suppression method, train-network power supply system.

I. INTRODUCTION

With the rapid development of electrified railways around the world, railway safety operations are getting more and more attention, especially in the train-network (''train-traction network'', which is referred to as ''train-network''). High-frequency resonance (HFR) and Low-frequency oscillation (LFO) are the main problems of train-network coupling instability, which have become urgent problems to be solved. The HFR usually occurs during the train operation. Some studies believe that under the action of harmonics, the traction power supply system and the train have the interaction of parameters such as inductance and capacitance, causing parallel and series resonance in the train-network system. The voltage and current in the train-network system increase exponentially, which leads to overvoltage and overcurrent [1]. The LFO exists mainly in occasions involving a train in rail depot. Some studies believe that with the increase of the number of electric trains, the total impedance of the train power system is reduced. When the total impedance is smaller than the traction network impedance, the system is in an unstable state, which is easy to cause LFO [2], [3]. The measured waveforms of typical HFR and LFO are shown in Figure 1. The characteristic of HFR is that the AC voltage and current contain a large amount of high-frequency harmonic components; the characteristic of LFO is that the DC voltage, AC voltage and current oscillate at the same frequency. The excessive voltage and current of serious HFR and LFO are easy to cause the train traction signal blocked or even damage the electrical equipment [4], [5].

At present, the HFR and LFO suppression methods are based on software or hardware. As for HFR, literature [6] suppresses the high-frequency harmonics generated by the train from the perspective of the train's internal network-side converter modulation strategy. An adaptive PWM algorithm is proposed. In the spectrum, the resonance frequency harmonics are eliminated, thereby suppressing the HFR phenomenon. Literature [7] adopts the method of installing the

The associate editor coordinating the review of this manuscript and approving it for publication was Sze Sing Lee.

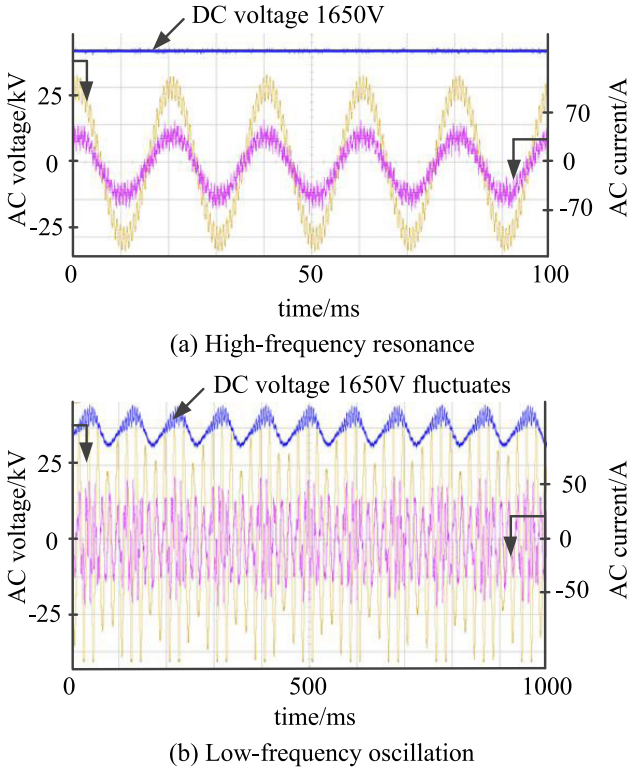

FIGURE 1. The measurement waveforms of HFR and LFO.

RC passive filter device on the front of the electric locomotive traction transformer, which suppresses the high-frequency harmonic injections to a certain extent. But due to the large size, high cost and lack of security of the RC passive filtering device, this scheme has not been widely used. As for LFO, literature [8] and [9] proposed multivariable control strategy, but this control strategy is completely different from the traditional double-closed control of voltage and current. The controller structure is complicated and it is difficult to implement. Moreover, the parameter design of this method has some difficulties [10]. In order to reduce the impedance of the traction network, literature [11] proposed a method. The original transformer of the substation is replaced by a transformer with a larger capacity and a smaller short-circuit voltage. But the hardware needs to be modified, which increases the cost and difficulty of the operation to some extent. At present, there are few measures have the ability to suppress both HFR and LFO. Our paper [12] proposed the active oscillation compensation (AOC) method which can suppress both HFR and LFO. The complexity of the software program is simplified, but this method requires a certain adjustment time in suppressing HFR, so it still needs to be improved.

Aiming at HFR and LFO phenomena, the VCT suppression method is proposed from the perspective of the network-side converter control strategy in this paper. Combined with the generalized Nyquist stability criterion and the dominant pole distribution analysis method, the effectiveness of VCT and AOC is theoretically analyzed. According to the suppression

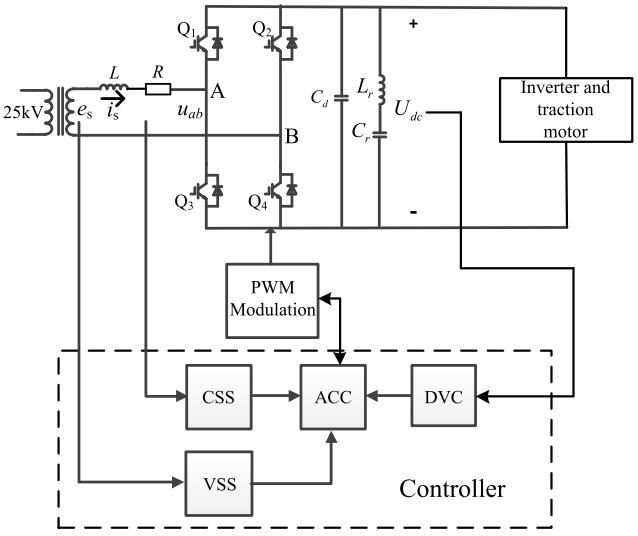

FIGURE 2. Controller of network-side converter.

characteristics of VCT and AOC, this paper further proposes the VCT-AOC comprehensive suppression method, which fully considers the type and degree of train-network coupling instability, and targeted rapid protection of the system. The VCT-AOC method is a further optimization of AOC suppression method.

The layout of this paper is as follows: the train-network impedance model is introduced briefly in Section II, which makes contributions to the analysis of the subsequent suppression methods; Section III mainly analyzes the suppression effect of AOC on HFR and LFO, and analyzes the reason why there is a long adjusting time when AOC suppresses HFR; the VCT-AOC comprehensive suppression method is proposed according to the characteristics of VCT and AOC in Section IV. In Section V, the effectiveness of suppression methods is verified through simulation and experiment; the conclusions are presented in Section VI.

II. THE IMPEDANCE MODEL OF THE TRAIN-NETWORK SYSTEM

A. THE IMPEDANCE MODEL OF THE TRAIN POWER SYSTEM

The model of the train has been thoroughly introduced in our paper [13], so only the conclusions that are needed by this paper are listed here as follows. The main transmission system structure diagram in the train is shown in Figure 2.

In order to make the network-side converter impedance model more accurate, the modeling process is divided into several parts: Voltage Synchronization System (VSS), Current Synchronization System (CSS), AC Current Controller (ACC) and DC Voltage Controller (DVC).

The impedance model of VSS is given as:

$$\underbrace{\begin{bmatrix}\Delta e_d^c\\ \Delta e_q^c\end{bmatrix}}_{\Delta e^c} = \underbrace{\begin{bmatrix}H_{edq} & G_{PLL}H_{edq}e_{q0}\\ 0 & H_{edq}-H_{edq}e_{d0}G_{PLL}\end{bmatrix}}_{G_{eVSS}} \underbrace{\begin{bmatrix}\Delta e_d\\ \Delta e_q\end{bmatrix}}_{\Delta e} \quad (1)$$

As for CSS, it gives:

$$\underbrace{\begin{bmatrix}\Delta i_d^c\\ \Delta i_d^c\end{bmatrix}}_{\Delta i^c} = \underbrace{\begin{bmatrix}H_{idq} & 0\\ 0 & H_{idq}\end{bmatrix}}_{H_{idq}}\underbrace{\begin{bmatrix}\Delta i_d\\ \Delta i_q\end{bmatrix}}_{\Delta i} - \underbrace{\begin{bmatrix}0 & -i_{q0}H_{idq}G_{PLL}\\ 0 & i_{d0}H_{idq}G_{PLL}\end{bmatrix}}_{G_{iCSS}}\underbrace{\begin{bmatrix}\Delta e_d\\ \Delta e_q\end{bmatrix}}_{\Delta e} \tag{2}$$

As for ACC, it gives:

$$\Delta i^c = G_{idqref}\,\Delta i_{ref} + G^c_{edq}\Delta e^c \tag{3}$$

where:

$$\begin{cases} G_{idqref} = (G^c_{dq})^{-1}G_{\mathrm{d}}K_{\mathrm{ACC}} \\ \Delta i_{ref} = \begin{bmatrix}\Delta i_{\mathrm{dref}}\\ \Delta i_{\mathrm{qref}}\end{bmatrix} \\ G^c_{edq} = (G^c_{dq})^{-1}(1-G_{\mathrm{d}}) \\ G^c_{dq} = \begin{bmatrix} G_{\mathrm{d}}K_{\mathrm{ACC}}+R+sL & \omega_0 L(G_{\mathrm{d}}-1) \\ -\omega_0 L(G_{\mathrm{d}}-1) & G_{\mathrm{d}}K_{\mathrm{ACC}}+R+sL\end{bmatrix} \end{cases} \tag{4}$$

Combining equation (1) and (2):

$$\Delta i = \underbrace{(H_{idq})^{-1}G_{idqref}}_{G_i}\Delta i_{ref} + \underbrace{(H_{idq})^{-1}(G_{iCSS}+G^c_{edq}G_{eVSS})}_{G_e}\Delta e \tag{5}$$

As for DVC, it gives:

$$\begin{bmatrix}\Delta i_{dref}\\ \Delta i_{qref}\end{bmatrix} = \underbrace{\begin{bmatrix}-K_{dvc}M_d & -K_{dvc}M_q\\ 0 & 0\end{bmatrix}}_{G_{ref}}\begin{bmatrix}\Delta e_d\\ \Delta e_q\end{bmatrix} \tag{6}$$

Finally, the train power system admittance expression can be obtained:

$$Y_{train} = G_i G_{ref} + G_e \tag{7}$$

B. THE IMPEDANCE MODEL OF TRACTION NETWORK

The model of traction network is divided into two parts: the impedance part and the admittance part. Among them, the impedance part is [14]:

$$\begin{bmatrix}\Delta u_{sd}\\ \Delta u_{sq}\end{bmatrix} = \begin{bmatrix}sL_s+R_s & -\omega_0 L_s\\ \omega_0 L_s & sL_s+R_s\end{bmatrix}\begin{bmatrix}\Delta i_{sd}\\ \Delta i_{sq}\end{bmatrix} \tag{8}$$

where, L_s and R_s are inductance and resistance of traction network. The subscript s represents traction network, d and q represents d axis and q axis. The angular frequency of the fundamental frequency is ω_0.

The admittance part is as follows:

$$\begin{bmatrix}\Delta i_{sd}\\ \Delta i_{sq}\end{bmatrix} = \begin{bmatrix}sC_s & -\omega_0 C_s\\ \omega_0 C_s & sC_s\end{bmatrix}\begin{bmatrix}\Delta u_{sd}\\ \Delta u_{sq}\end{bmatrix} \tag{9}$$

where, C_s is the equivalent capacitance of traction network.

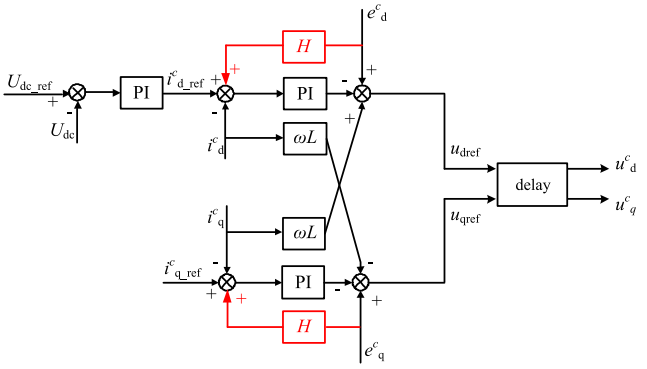

FIGURE 3. The control block diagram of network-side converter with AOC.

The impedance of the network Z_{g} is shown as follows:

$$Z_s = \left(\begin{bmatrix}sL_s+R_s & -\omega_0 L_s\\ \omega_0 L_s & sL_s+R_s\end{bmatrix}^{-1} + \begin{bmatrix}sC_s & -\omega_0 C_s\\ \omega_0 C_s & sC_s\end{bmatrix}\right)^{-1} \tag{10}$$

III. THE ANALYSIS OF THE SUPPRESSION EFFECT OF AOC ON HFR AND LFO

A. THE BASIC PRINCIPLE OF AOC METHOD

The active oscillation compensation suppression method is implemented by collecting the input voltage e_{s} of the network-side converter, performing dq conversion, obtaining DC quantities $e^{\mathrm{c}}_{\mathrm{d}}$ and $e^{\mathrm{c}}_{\mathrm{q}}$, passing through a high-pass filter with a low cutoff frequency, filtering out the DC amount, and obtaining the oscillation components. The oscillation components are compensated to the current loop of the network-side converter, thereby weakening the oscillation. The block diagram of the network-side converter with AOC suppression is shown in Figure 3.

Since the oscillations contain both high-frequency components and low-frequency components, the AOC suppression method has a suppressive effect on both HFR and LFO.

The H in Figure 3 is a virtual high-pass filter (VHPF) whose main purpose is to separate the DC quantities in $e^{\mathrm{c}}_{\mathrm{d}}$ and $e^{\mathrm{c}}_{\mathrm{q}}$, taking out the oscillation components. Then, the oscillation components are compensated to the current loop of the network-side converter. Due to the $i^{\mathrm{c}}_{\mathrm{d}}$ and $i^{\mathrm{c}}_{\mathrm{q}}$ also have oscillation components, and these components can be weakened by the oscillation compensation method, so that the train-network system can return to a stable state.

Here, the first-order VHPF is selected as the research object, and the expression of $H_1(s)$ in the s domain is:

$$H_1(s) = \frac{s}{s+\omega_{\mathrm{c}}} \tag{11}$$

where $\omega_{\mathrm{c}} = 2\pi f_{\mathrm{c}}$ is the cutoff angle frequency, and f_{c} is the cutoff frequency. Different cut-off frequencies are correspondence with different time delay of H_1. The Bode diagram with different cut-off frequencies (different time delay) is shown in Figure 4. It can be seen that the larger the f_{c}, the larger the time delay.

Since the DC component needs to be filtered out, the oscillation component is retained, so $f_{\mathrm{c}} = 1$ Hz. The influence of different time delay on the system is analyzed in part B.

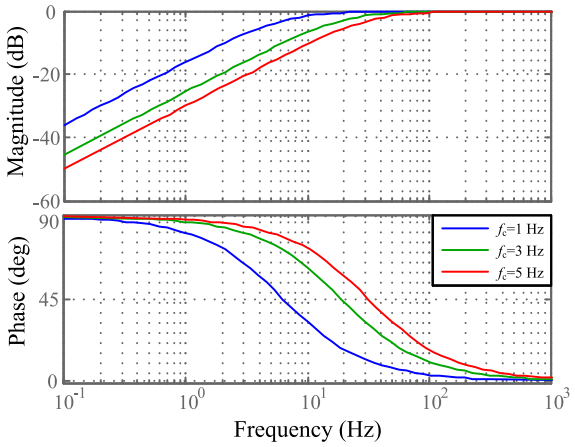

FIGURE 4. The Bode diagram of H_1 with different f_c.

The train power system impedance modeling process after taking AOC suppression method is as follows:

$$\begin{bmatrix} \Delta u_{\mathrm{d}}^{\mathrm{c}} \\ \Delta u_{\mathrm{q}}^{\mathrm{c}} \end{bmatrix} = \begin{bmatrix} \Delta e_{\mathrm{d}}^{\mathrm{c}} \\ \Delta e_{\mathrm{q}}^{\mathrm{c}} \end{bmatrix} - \begin{bmatrix} R+sL & -\omega_0 L \\ \omega_0 L & R+sL \end{bmatrix} \begin{bmatrix} \Delta i_{\mathrm{d}}^{\mathrm{c}} \\ \Delta i_{\mathrm{q}}^{\mathrm{c}} \end{bmatrix} \quad (12)$$

The current loop is controlled by the PI part and decoupling control, so as to obtain the command value of the modulated wave in dq rotating coordinate system:

$$\begin{bmatrix} \Delta u_{\mathrm{dref}} \\ \Delta u_{\mathrm{qref}} \end{bmatrix} = \begin{bmatrix} \Delta e_{\mathrm{d}}^{\mathrm{c}} \\ \Delta e_{\mathrm{q}}^{\mathrm{c}} \end{bmatrix} - K_{\mathrm{ACC}} \begin{bmatrix} \Delta i_{\mathrm{dref}} - \Delta i_{\mathrm{d}}^{\mathrm{c}} - H_1(s)\Delta e_{\mathrm{d}}^{\mathrm{c}} \\ \Delta i_{\mathrm{qref}} - \Delta i_{\mathrm{q}}^{\mathrm{c}} - H_1(s)\Delta e_{\mathrm{q}}^{\mathrm{c}} \end{bmatrix} - \begin{bmatrix} 0 & -\omega_0 L \\ \omega_0 L & 0 \end{bmatrix} \begin{bmatrix} \Delta i_{\mathrm{d}}^{\mathrm{c}} \\ \Delta i_{\mathrm{q}}^{\mathrm{c}} \end{bmatrix} \quad (13)$$

The modulated wave command value is delayed to obtain the modulated wave controlled quantities:

$$\begin{bmatrix} \Delta u_{\mathrm{d}}^{\mathrm{c}} \\ \Delta u_{\mathrm{q}}^{\mathrm{c}} \end{bmatrix} = G_{\mathrm{d}} \begin{bmatrix} \Delta u_{\mathrm{dref}} \\ \Delta u_{\mathrm{qref}} \end{bmatrix} \quad (14)$$

where, $G_{\mathrm{d}} = 1/(T_{\mathrm{d}}s+1)$ is the delay part.

Combining equations (12)∼(14):

$$\boldsymbol{\Delta i^c} = \boldsymbol{G_{\mathrm{idqref}}} \boldsymbol{\Delta i_{\mathrm{ref}}} + \boldsymbol{G_{\mathrm{edq}}^c} \boldsymbol{\Delta e^c} \quad (15)$$

where:

$$\begin{cases} \boldsymbol{G_{\mathrm{idqref}}} = (\boldsymbol{G_{\mathrm{dq}}^c})^{-1} G_{\mathrm{d}} K_{\mathrm{ACC}} \\ \boldsymbol{\Delta i_{\mathrm{ref}}} = \begin{bmatrix} \Delta i_{\mathrm{dref}} \\ \Delta i_{\mathrm{qref}} \end{bmatrix} \\ \boldsymbol{G_{\mathrm{edq}}^c} = (\boldsymbol{G_{\mathrm{dq}}^c})^{-1}(1 - G_{\mathrm{d}} - G_{\mathrm{d}} K_{\mathrm{ACC}} H_1(s)) \\ \boldsymbol{G_{\mathrm{dq}}^c} = \begin{bmatrix} G_{\mathrm{d}} K_{\mathrm{ACC}} + R + sL & \omega_0 L(\boldsymbol{G}_{\mathrm{d}} - 1) \\ -\omega_0 L(G_{\mathrm{d}} - 1) & G_{\mathrm{d}} K_{\mathrm{ACC}} + R + sL \end{bmatrix} \end{cases} \quad (16)$$

Substituting equation (16) with equation (4), the admittance model of the train power system with AOC suppression method can be obtained.

B. ANALYSIS OF AOC ON THE STABILITY OF TRAIN-NETWORK SYSTEM

It can be seen from literature [15] that the train-network system can be represented as a small-signal multivariable

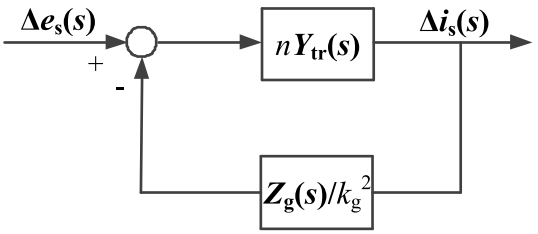

FIGURE 5. Multivariable closed loop feedback system of train-network.

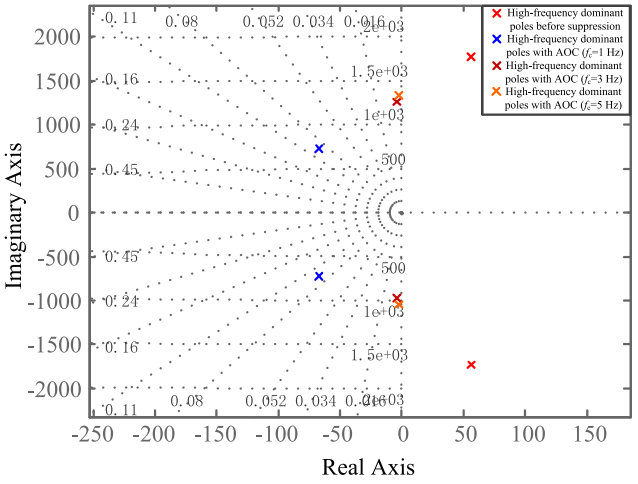

FIGURE 6. The dominant poles diagram of the system with different time delay of H_1.

closed-loop feedback system, as shown in Figure 5. The input of the feedback system is the secondary side voltage $\Delta \boldsymbol{e_s}(\boldsymbol{s})$ of the onboard traction transformer, and the output is the train input current $\Delta \boldsymbol{i_s}(\boldsymbol{s})$.

Where, $\boldsymbol{Z_g}(\boldsymbol{s})/k_{\mathrm{g}}^2$ is the impedance of the traction network on the secondary side of the on-board traction transformer, and k_{g} is the turns ratio of traction transformer. The train power system admittance is $\boldsymbol{Y_{tr}}(\boldsymbol{s})$, and n is the number of network-side converter modules. According to literature [16] and [17], the closed-loop transfer function of the system is:

$$\boldsymbol{H_s} = (s) \frac{n\boldsymbol{Y_{\mathrm{tr}}}(\boldsymbol{s})}{\mathbf{I}_{2\times 2} + n\boldsymbol{Y_{\mathrm{tr}}}(\boldsymbol{s}) \cdot \frac{\boldsymbol{Z_g}(\boldsymbol{s})}{k_{\mathrm{g}}^2}} \quad (17)$$

Among them, the bold font indicates a matrix form; $\mathrm{I}_{2\times 2}$ is a 2×2 unit matrix.

In fact, different time delay of the high-pass filter has different influence on the system, and different cut-off frequencies are correspondence with different time delay. It is necessary to analyze the dominant pole distribution under different time delay, which is shown in Figure 6. It shows that when $f_{\mathrm{c}} = 3$ and 5 Hz, the dominant poles are too close to the imaginary axis, that is to say, the suppression effect is not good enough.

When $L_{\mathrm{g}} = 3.85$ mH, the train-network system is in HFR state before AOC suppression method is taken. After obtaining AOC method, the system becomes stable again. The generalized Nyquist comparison diagrams of the

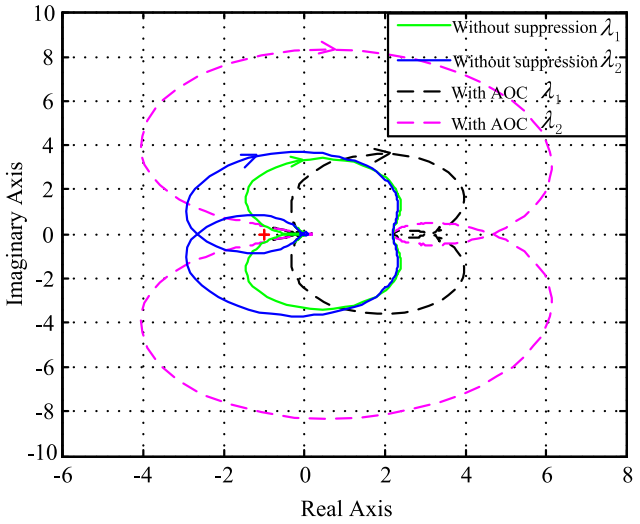

FIGURE 7. The generalized Nyquist diagram of the system with and without AOC method when L_g. =3.85 mH.

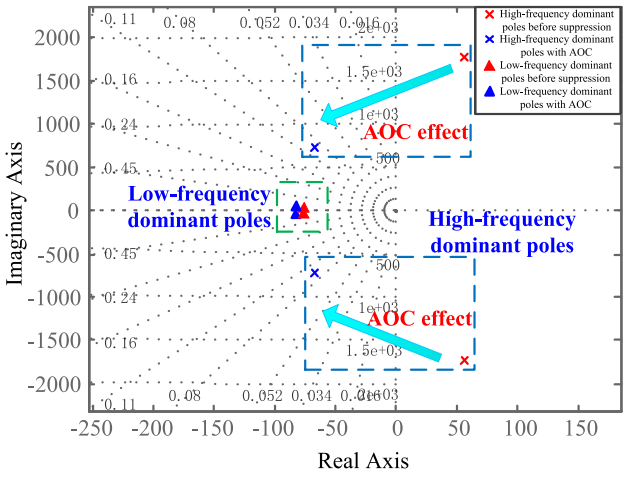

FIGURE 8. The dominant poles diagram of the system with and without AOC method when L_g = 3.85 mH.

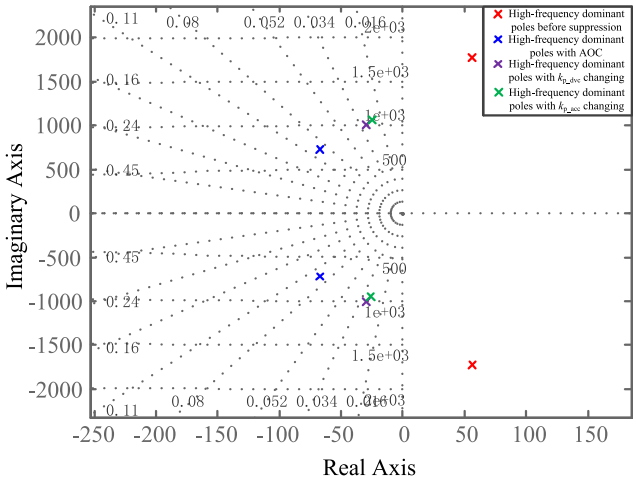

FIGURE 9. The dominant poles diagram of the system with and without PI changing when L_g = 3.85 mH.

train-network system with and without AOC are shown in Figure 7. As can be seen from Figure 7, without AOC suppression method, the eigenvalue trajectory of the system is clockwise surrounded $(-1, j0)$ point, so the system is in an unstable state. When AOC suppression method is adopted, the system does not surround $(-1, j0)$ point, the system becomes stable again.

The suppression effect of HFR by AOC suppression method is analyzed from the perspective of the dominant poles of the closed-loop transfer function of the train-network system, as shown in Figure 6. When $L_g = 3.85$ mH, the HFR phenomenon occurs, and the high-frequency dominant poles are distributed in the right half-plane, and the high-frequency damping ratio of the system is negative. The low-frequency dominant poles are distributed in the left half-plane. After obtaining AOC suppression method, the high-frequency dominant poles move to the left half plane, and the high-frequency damping ratio ξ of the system is about 0.09, the system becomes stable again, and the low-frequency dominant poles only change slightly. The reason for this change is that when $L_g = 3.85$ mH, the HFR phenomenon occurs, and e_d^c and e_q^c contain a large amount of high-frequency harmonic components, while low-frequency oscillation components are small. Through the high-pass filter, these high-frequency harmonic components are compensated into the current loop, and the high-frequency characteristic of the system is improved. It is worth noting that PI parameters also have a certain impact on system damping. Due to the integral parameters of the voltage loop and current loop have less influence on the system [18], only the voltage and current loop proportional parameters (k_{p_dvc} and k_{p_acc}) are analyzed in this paper. The influence of k_{p_dvc} and k_{p_acc} changing on the system damping is shown in Figure 9. Reducing k_{p_dvc} and increasing k_{p_acc} appropriately can make the system stable. The high-frequency dominant poles move to the left half plane, but the high-frequency damping ratio ξ of the system is between 0.02 and 0.034, which is less than the damping ration when AOC method is adopted. What's more, the PI parameters can only be adjusted in a limited range, it cannot be used as a long-term solution. Therefore, this paper mainly suppresses the unstable phenomena from the perspective of changing the control structure like AOC and VCT (mentioned in IV) methods.

When $L_g = 31.5$ mH, the train-network system is in the LFO state before the AOC suppression method is taken. The generalized Nyquist figure of the train-network system is shown in Figure 10. It can be seen from the figure that without AOC suppression method, the eigenvalue trajectory of the system is clockwise surrounded $(-1, j0)$ point, and the system is unstable. When the AOC suppression method is adopted, the system does not surround $(-1, j0)$ point, the system becomes stable again.

The suppression effect of LFO by AOC suppression method is analyzed from the perspective of the dominant poles of the closed-loop transfer function of the train-network

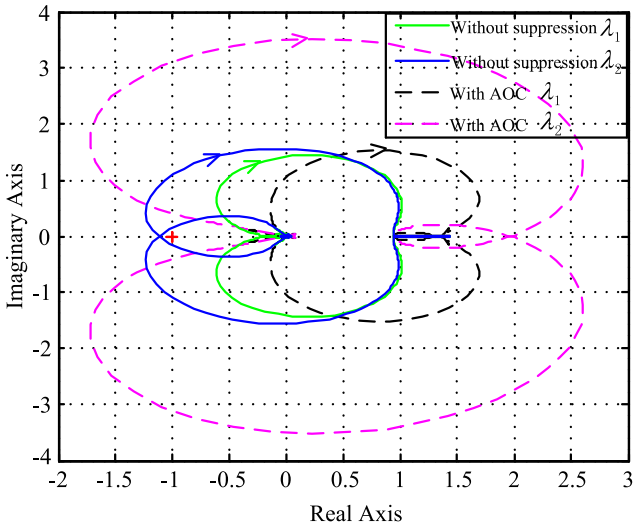

FIGURE 10. The generalized Nyquist diagram of the system with and without AOC method when $L_g = 31.5$ mH.

system, as shown in Figure 11 (a) (b), where figure (b) is the magnified figure of figure (a). When $L_g = 31.5$ mH, the LFO occurs. The low-frequency dominant poles are distributed in the right half-plane, and the low-frequency damping ratio of the system is negative. The high-frequency dominant poles are distributed in the left half-plane. When the AOC suppression method is taken, the low-frequency dominant poles move to the left half plane, and the low-frequency damping ratio ξ of the system is about 0.78, the system becomes stable again. The high-frequency dominant poles only change slightly. The reason for this change is that when $L_g = 31.5$ mH, the LFO phenomenon occurs, and e_d^c and e_q^c contain a large number of low-frequency oscillation components, and high-frequency harmonic components are small. Through the high-pass filter, these low-frequency oscillation components are compensated into the current loop, and the low-frequency characteristic of the system is improved. Similar to HFR, although adjusting the PI parameters can stabilize the system, the system damping is small.

Although the AOC suppression method has suppressing effects on both HFR and LFO, the adjustment time for HFR is a little bit long. From the comparative study of Figure 6 and Figure 11, it is found that the dominant poles shifted to the left by the AOC method, but the distance from the imaginary axis is smaller than the original low-frequency oscillation system (the system corresponding to Figure 11). The simulation study also reached the same conclusion. As shown in Figure 12, when the equivalent inductance of the traction network is 3.85 mH, the HFR happened. The AOC method is adopted at 1 s. The THD of the network-side voltage e_g measured from 0.4s for 30 fundamental periods is as high as 21.74%, which is shown in Figure 13; the THD of e_g measured from 1.08 s for 30 fundamental periods is still as high as 17.20%, which is shown in Figure 14. The THD of e_g measured from 1.4 s for 30 fundamental periods is 1.23%, which is shown in Figure 15. Studies show

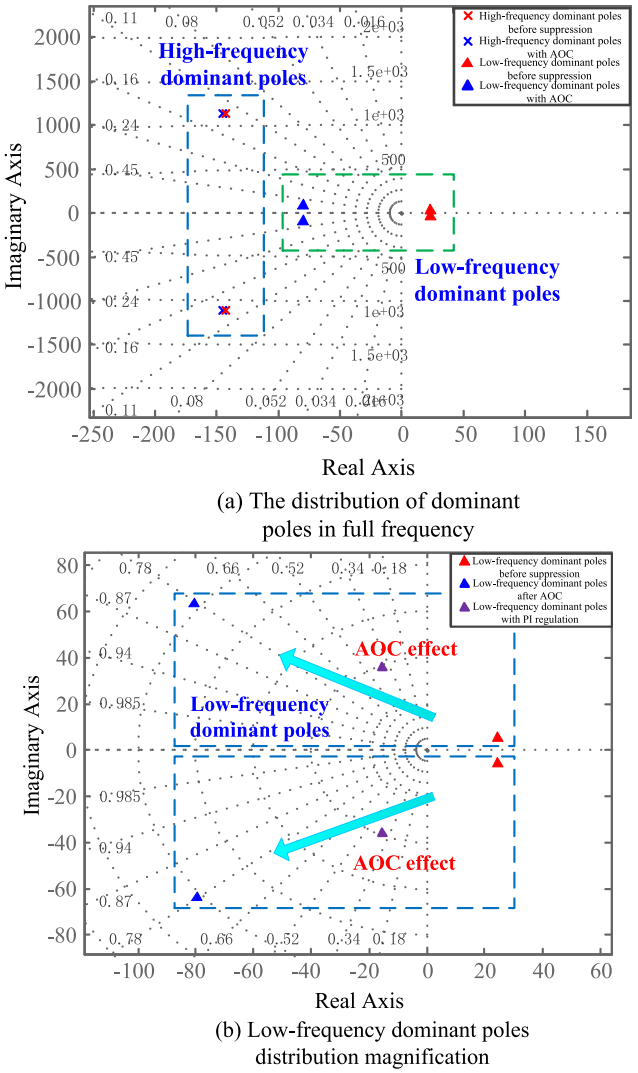

FIGURE 11. The dominant poles diagram of the system with and without AOC method when $L_g = 31.5$ mH.

that when serious HFR occurs, the adjustment time of AOC suppression method will be longer. In order to improve this shortcoming of AOC, other auxiliary suppression method is needed.

IV. VCT-AOC COMPREHENSIVE SUPPRESSION METHOD

A. THE PRINCIPLE OF VCT SUPPRESSION METHOD

When the network-side converter is in a steady state, the *dq* transform components e_d^c and e_q^c of the network voltage are constant quantities. Since e_d^c and e_q^c are per units, $e_d^c = 1$, $e_q^c = 0$. When HFR occurs in the train-network system, e_d^c and e_q^c also contain high-frequency harmonics [19]. If a more severe resonance is introduced into the control, the current resonance will be aggravated, causing the voltage loop and the current loop to be "overstressed" and losing the adjustment capability, resulting in severe HFR in the entire system. In order to reduce the hazard of resonance, we made $e_d^c = 1$, $e_q^c = 0$, forcing to remove the resonance components in the

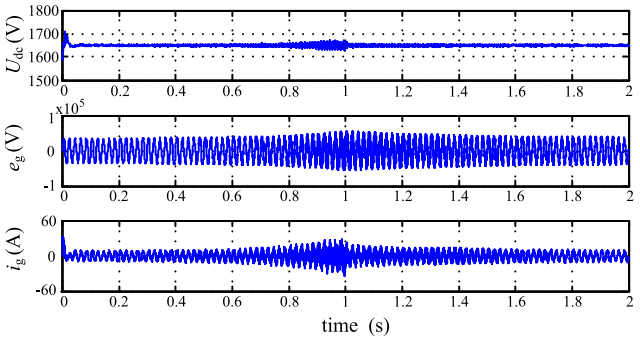

FIGURE 12. The simulation waveforms of HFR.

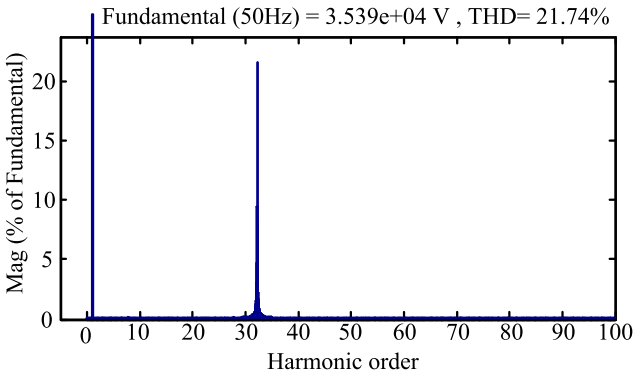

FIGURE 13. The THD of the primary side voltage of traction transformer without AOC.

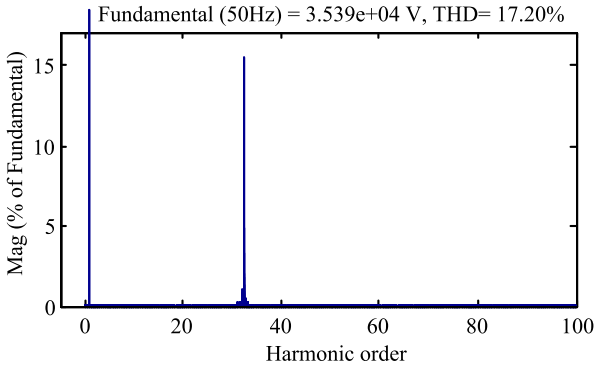

FIGURE 14. The THD of the primary side voltage of traction transformer with AOC (start from 1.08 s).

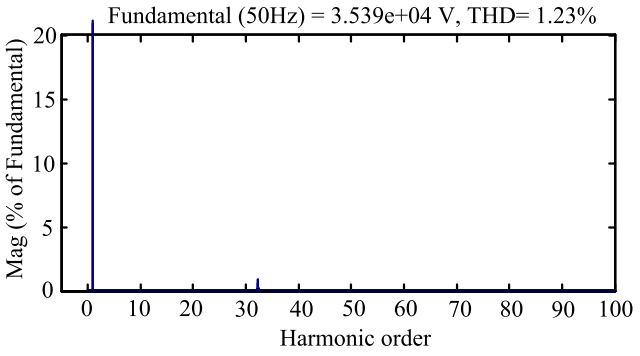

FIGURE 15. The THD of the primary side voltage of traction transformer with AOC (start from 1.4 s).

network voltage, thereby reducing the control difficulties of the voltage loop and the current loop.

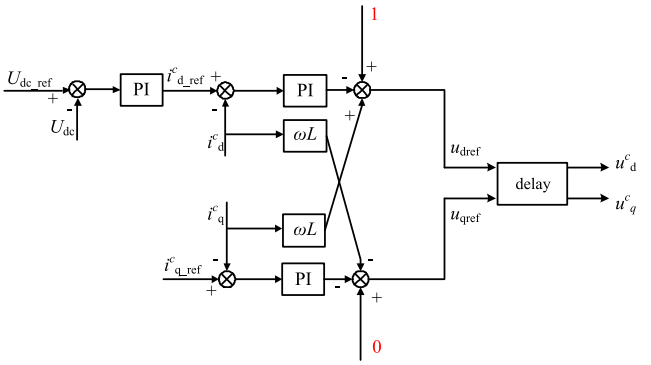

FIGURE 16. The control block diagram of network-side converter with VCT.

The block diagram of the network-side converter with VCT suppression method is shown in Figure 16.

The train power system impedance modeling process with VCT suppression method is as follows. Since $e_d^c = 1$ and $e_q^c = 0$, Δe_d^c and Δe_q^c are both 0.

$$\begin{bmatrix} \Delta u_d^c \\ \Delta u_q^c \end{bmatrix} = -\begin{bmatrix} R + sL & -\omega_0 L \\ \omega_0 L & R + sL \end{bmatrix} \begin{bmatrix} \Delta i_d^c \\ \Delta i_q^c \end{bmatrix} \tag{18}$$

The current loop is controlled by the PI part and decoupling to obtain the command value of the modulated wave in *dq* rotating coordinate system:

$$\begin{bmatrix} \Delta u_{dref} \\ \Delta u_{qref} \end{bmatrix} = -K_{ACC} \begin{bmatrix} \Delta i_{dref} - \Delta i_d^c \\ \Delta i_{qref} - \Delta i_q^c \end{bmatrix} - \begin{bmatrix} 0 & -\omega_0 L \\ \omega_0 L & 0 \end{bmatrix} \begin{bmatrix} \Delta i_d^c \\ \Delta i_q^c \end{bmatrix} \tag{19}$$

The modulated wave control quantities can be obtained:

$$\begin{bmatrix} \Delta u_d^c \\ \Delta u_q^c \end{bmatrix} = G_d \begin{bmatrix} \Delta u_{dref} \\ \Delta u_{qref} \end{bmatrix} \tag{20}$$

Combining equation (18)∼(20):

$$\boldsymbol{\Delta i^c} = \boldsymbol{G_{idqref}} \boldsymbol{\Delta i_{ref}} + \boldsymbol{G^c_{edq}} \boldsymbol{\Delta e^c} \tag{21}$$

where:

$$\begin{cases} \boldsymbol{G_{idqref}} = (\boldsymbol{G^c_{dq}})^{-1} G_d K_{ACC} \\ \boldsymbol{\Delta i_{ref}} = \begin{bmatrix} \Delta i_{dref} \\ \Delta i_{qref} \end{bmatrix} \\ \boldsymbol{G^c_{edq}} = 0 \\ \boldsymbol{G^c_{dq}} = \begin{bmatrix} G_d K_{ACC} + R + sL & \omega_0 L(\boldsymbol{G}_d - 1) \\ -\omega_0 L(G_d - 1) & G_d K_{ACC} + R + sL \end{bmatrix} \end{cases} \tag{22}$$

Substituting equation (22) for equation (4), the admittance model of train power system with VCT suppression method can be obtained.

B. THE ANALYSIS OF THE SUPPRESSION EFFECT OF VCT ON HFR

When $L_g = 4.36$ mH, the train-network system has a more serious HFR phenomenon before taking any

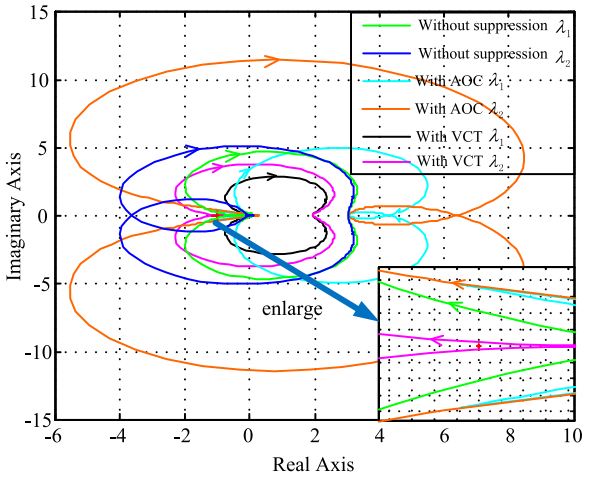

FIGURE 17. The generalized Nyquist diagram of the system with and without VCT or AOC method when $L_g = 4.36$ mH.

suppression methods. After taking the VCT or AOC suppression methods, the generalized Nyquist comparison diagrams of the train-network system are shown in Figure 17.

As can be seen from Figure 17, when the system does not take any suppression methods, the eigenvalue trajectory of the system is clockwise surrounded $(-1, j0)$, and the system is unstable. When AOC or VCT suppression methods are taken, the system does not surround $(-1, j0)$ point, the system returns to a steady state.

The suppression effect of HFR by VCT suppression method is analyzed from the perspective of the dominant poles of the closed-loop transfer function of the train-network system, as shown in Figure 18 (a) (b). When $L_g = 4.36$ mH, the train-network system has a serious HFR phenomenon (which is shown in Part V). The high-frequency dominant poles are distributed in the right half plane, and the system's high-frequency damping ratio is negative. The low-frequency dominant poles are distributed in the left half plane. When the VCT suppression method is taken, the high frequency dominant poles move to the left half plane, and the system's high frequency damping ratio is about 0.052, and the system becomes stable again. At the same time, the low frequency dominant poles shift to the left and the damping ratio decreases. Comparing with the AOC suppression method, the VCT suppression method can make the dominant poles farther from the imaginary axis and shorten the adjustment time t_s to some extent. But the system's high and low frequency damping ratios are smaller than the corresponding damping ratios of the system with AOC suppression method. As for high frequency, VCT suppression method has the advantage of making the system recover quickly, but reduce the system damping. As for low frequency, the system already has appropriate damping ratio and adjustment time when adopting AOC method. The VCT method only makes the system "sacrifices" the damping ratio while further reducing the adjustment time, so it is not desirable. In summary, the VCT suppression method is only used as a temporary suppression

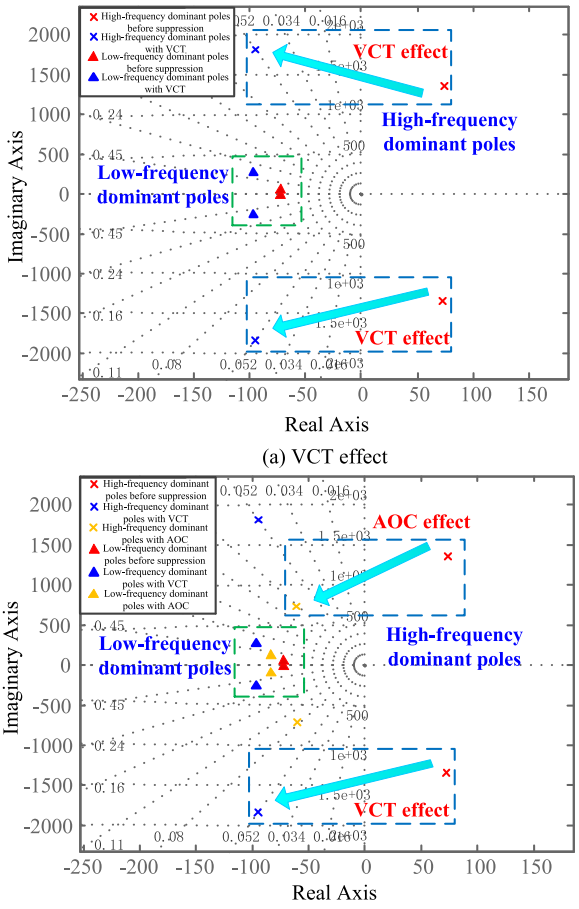

FIGURE 18. The dominant poles diagram of the system with and without VCT method when $L_g = 4.36$ mH.

mean for HFR. After the system is quickly restored and stabilized, the AOC suppression method still needs to be adopted, and the system damping ratio is improved on the basis of shortening the adjustment time. The low-frequency characteristic is also optimized.

C. THE IMPLEMENTATION PLAN OF VCT-AOC COMPREHENSIVE SUPPRESSION METHOD

It can be seen from the above that the AOC suppression method can suppress both HFR and LFO phenomena occurring in the train-network system, but if the system has a severe HFR, the AOC suppression method requires a long adjustment time to stabilize the system. In this case, it is necessary to assist VCT suppression method, so the voltage constant transient active oscillation compensation (VCT-AOC) comprehensive suppression method is proposed.

This method requires the train-network system to detect the network voltage in real time to determine whether the system has instability and what type of instability has occurred. The system frequency needs to be detected in real time to determine if HFR or LFO happens. The method for detecting the resonance or oscillation frequency is given in literature [20] and [21]. It will not be described here. The system also

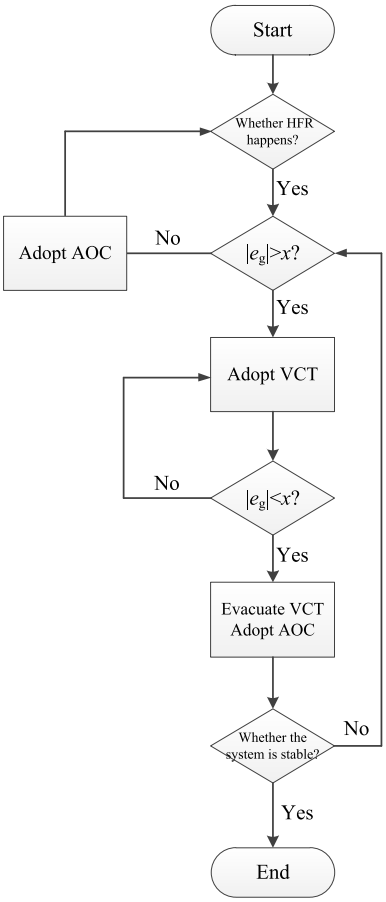

FIGURE 19. The flow chart of VCT-AOC comprehensive suppression method.

needs to detect the amplitude of the resonance of the network voltage when HFR happens, in order to judge whether it is necessary to adopt VCT suppression method to assist the system become stable quickly. The VCT-AOC comprehensive suppression method needs the system to be divided into two situations, and different schemes are adopted according to different situations:

(1) The system is stable or LFO occurs: the AOC suppression method is applied;

(2) The HFR occurs in the system: if the system detects that the network voltage resonance amplitude is greater than x (x can be determined according to the actual situation), the VCT suppression method is applied, and the resonance amplitude will reduce rapidly. When the resonance amplitude is less than x, the VCT will be evacuated and the AOC will be adopted. If the HFR happens again, repeat the above steps until the system is stable.

The above is the implementation plan of the VCT-AOC comprehensive suppression method, and its execution flow is shown in Figure 19.

V. SIMULATIONS AND EXPERIMENTS

The VCT-AOC suppression method is verified by the train-network joint Matlab simulation and semi-physical experiment using Typhoon HIL 602. Referring our paper [22], the simulation and experimental parameters are shown in Table 1.

TABLE 1. Simulation and experiment parameters.

Symbols	Note	Simulation Value	Experiment Value
e_g	The voltage of catenary	25 kV	25 kV
U_{dc}	DC voltage	1650 V	1650 V
L	Leakage inductance of transformer	2.08 mH	2.08 mH
R	Leakage resistance of transformer	0.2 Ω	0.2 Ω
L_g	Network equivalent inductance	4.36 mH for HFR; 31.5 mH for LFO	4.51 mH for HFR; 32.7 mH for LFO
R_g	Network equivalent resistance	0.1 Ω	0.1 Ω
C_g	Network equivalent capacitance	2.8 μF	2.75 μF
C_d	Capacitance in DC side	8 mF	8 mF
L_r	Secondary resonance inductance	0.359 mH	0.359 mH
C_r	Secondary resonance capacitance	7.06 mF	7.06 mF

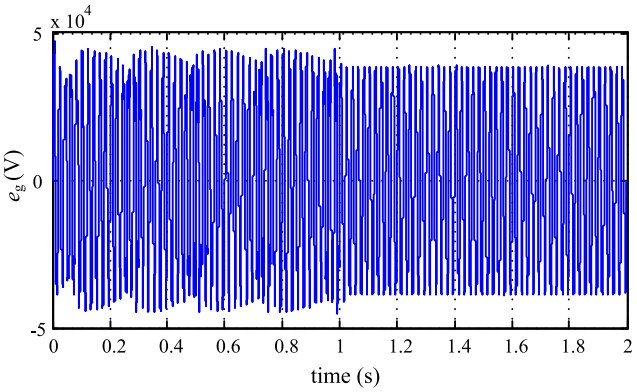

FIGURE 20. The simulation waveform of LFO with AOC.

A. SIMULATION VERIFICATION

When the traction network inductance is 31.5 mH, the network voltage e_g appears a revere LFO phenomenon, and the AOC suppression method is added at 1 s. The simulated waveform of e_g is shown in Figure 20.

Starting from 0.4 s, the THD of network voltage e_g for 30 fundamental periods is measured. The FFT analysis is shown in Figure 21. The THD is as high as 28.65%.

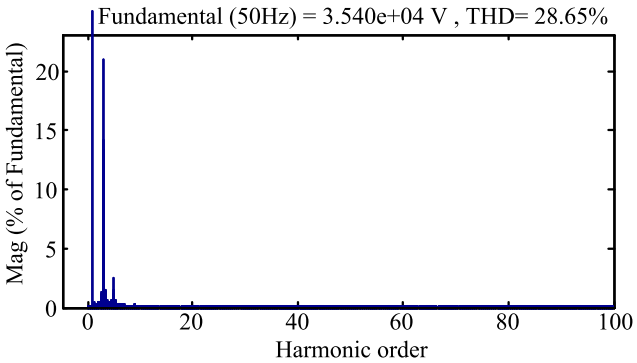

FIGURE 21. The THD of the primary side voltage of traction transformer without AOC.

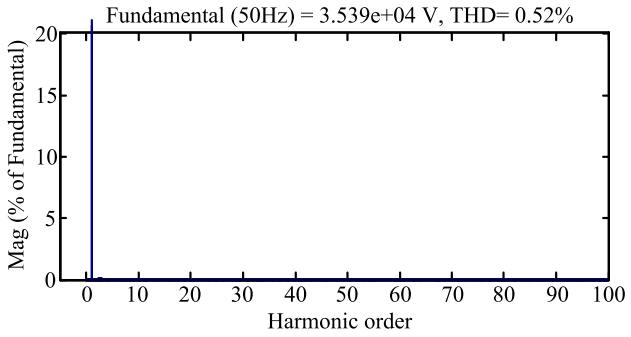

FIGURE 22. The THD of the primary side voltage of traction transformer with AOC.

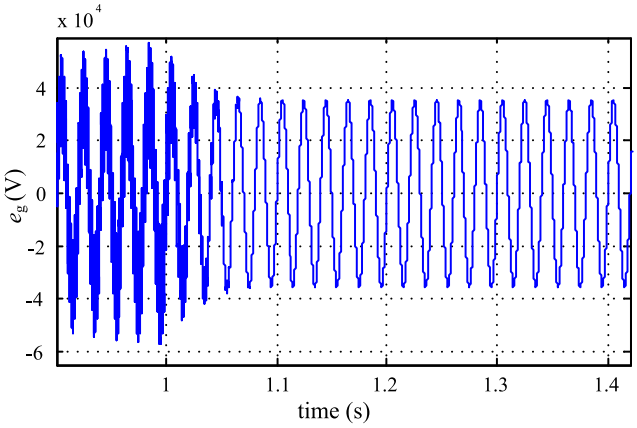

FIGURE 23. The simulation waveform of HFR with VCT.

After adopting the AOC suppression method, the THD of network voltage e_g for 30 fundamental periods is measured from the time of 1.04 s, and the FFT analysis is as shown in Figure 22. The THD is reduced to 0.52%.

When the traction network inductance is 4.36 mH, the network voltage e_g has a serious HFR phenomenon. The VCT suppression method is added at 1 s. The simulated waveform of e_g is shown in Figure 23.

As can be seen from Figure 23, after adopting the VCT suppression method at 1 s, the network voltage e_g becomes normal again from the fourth fundamental frequency cycle.

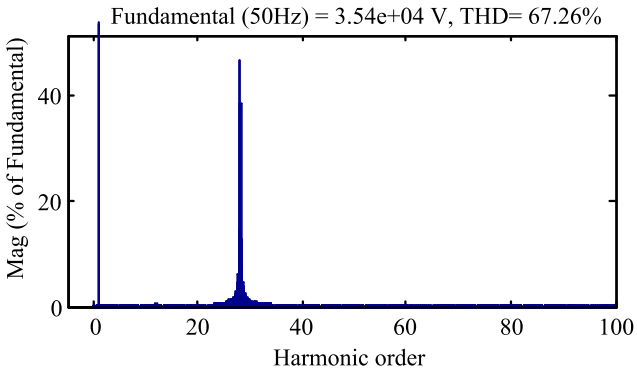

FIGURE 24. The THD of the primary side voltage of traction transformer without VCT.

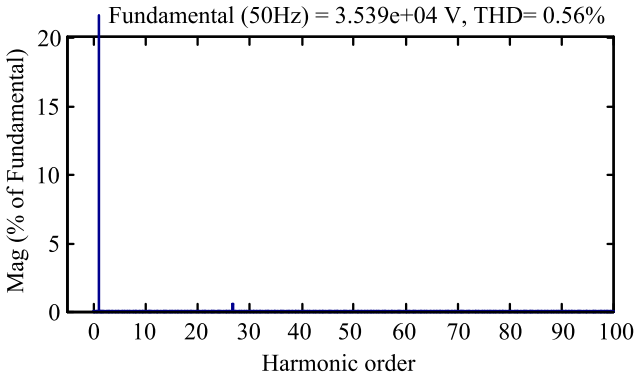

FIGURE 25. The THD of the primary side voltage of traction transformer with VCT.

Starting from 0.4 s, the THD of network voltage e_g for 30 fundamental periods is measured. The FFT analysis is shown in Figure 24. The THD is as high as 67.26%.

After adopting the VCT suppression method, the THD of network voltage e_g for 30 fundamental periods is measured from 1.08 s. The FFT analysis is shown in Figure 25. After adopting VCT suppression method, the THD of e_g is reduced to 0.56%. Compared with Figure 14, the THD of e_g measured from 1.08 s for 30 fundamental periods is still as high as 17.20% with the AOC suppression method. That is to say, when serious HFR happens, the VCT method is better than the AOC method.

B. EXPERIMENTAL VERIFICATION

The VCT-AOC suppression method is also verified by the Typhoon HIL 602 semi-physical simulation platform. The picture of experimental console is in Figure 26.

When LFO happens, adopting AOC suppression method, the waveforms of DC voltage, AC voltage and current are shown in Figure 27.

The AOC suppression method is adopted in point M. It can be seen from the Figure 27 that LFO occurs in e_g, i_g and U_{dc} before M. After the system adopting AOC suppression method, the system returns to steady state in the next oscillation cycle. The experiment results further illustrates that AOC suppression method can suppress LFO quickly and effectively.

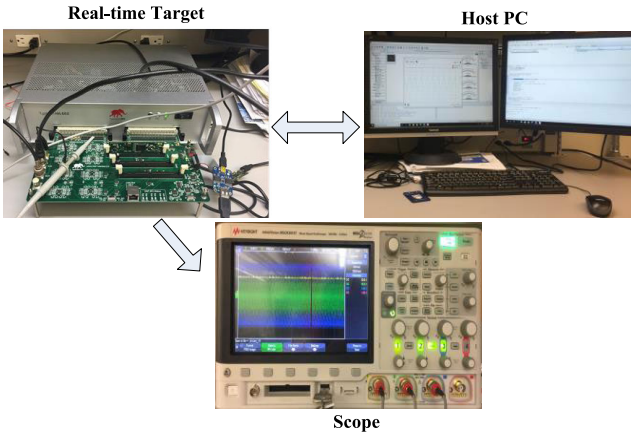

FIGURE 26. The experimental platform based on Typhoon HIL 602.

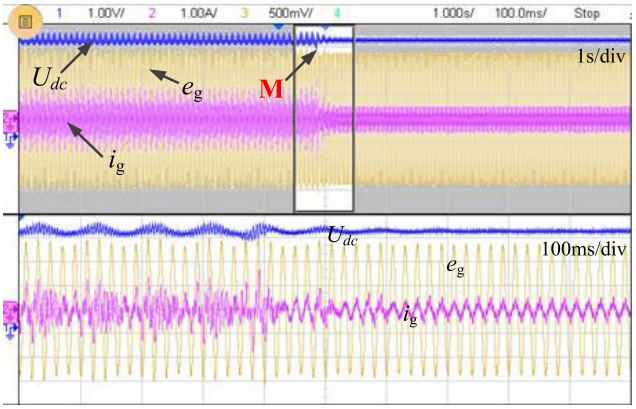

FIGURE 27. The experimental waveforms of LFO with AOC.

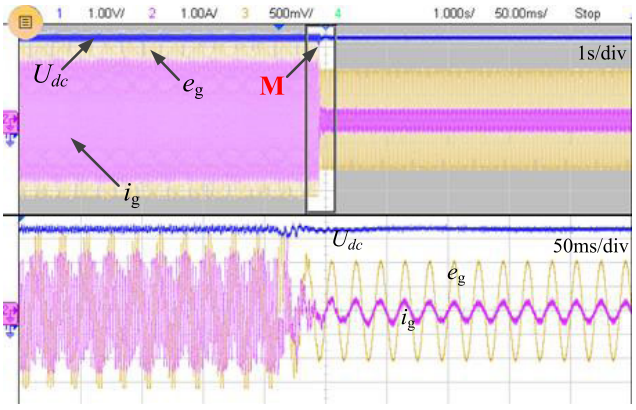

FIGURE 28. The experimental waveforms of HFR with VCT.

When severe HFR happens, adopting VCT suppression method, the DC voltage, AC voltage, and current waveforms are shown in Figure 28.

The VCT suppression method is adopted in point M. It can be seen from the Figure 28 that the high-frequency harmonics of e_g and i_g are high before point M. After adopting VCT suppression method, the network voltage e_g becomes normal again from the third fundamental frequency cycle. The experiment results further demonstrates that VCT suppression method can suppress more severe HFR phenomena quickly and effectively. The AOC method is good at suppressing LFO. The VCT method is good at suppressing severe HFR. Combined with the characteristics of AOC and VCT, the VCT-AOC comprehensive suppression scheme can cope with the train-network system coupled instability phenomena effectively.

VI. CONCLUSION

In this paper, VCT suppression method is proposed aiming at shortening adjustment time. This method can make the system become stable quickly by removing the network voltage oscillation in the converter control completely. By comparing the generalized Nyquist figures and the dominant poles distribution figures of train-network system with and without AOC and VCT suppression methods, the characteristics of AOC and VCT are summarized. VCT can shorten the adjustment time and protect the system quickly, but the system damping is relatively low. The AOC suppression method can give the system an appropriate damping ratio. According to the characteristics of AOC and VCT suppression methods, the VCT-AOC comprehensive suppression method is proposed and the specific implementation plan of this method is given in this paper. The VCT-AOC method fully considers the type and degree of train-network coupling instability of the train-network system, and targeted rapid protection of the system, avoiding the damage of HFR and LFO to the system. The VCT-AOC method is a further optimization of AOC suppression method.

REFERENCES

[1] H. Hu, Y. Shao, L. Tang, J. Ma, Z. He, and S. Gao, "Overview of harmonic and resonance in railway electrification systems," *IEEE Trans. Ind. Appl.*, vol. 54, no. 5, pp. 5227–5245, Sep./Oct. 2018.

[2] C. Heising, R. Bartelt, M. Oettmeier, V. Staudt, and A. Steimel, "Improvement of low-frequency system stability in 50-Hz railway-power grids by multivariable line-converter control in a distance-variation scenario," in *Proc. Elect. Syst. Aircr., Railway Ship Propuls.*, Bologna, Italy, Oct. 2010, pp. 1–5.

[3] H. Cui, W. Song, H. Fang, X. Ge, and X. Feng, "Resonant harmonic elimination pulse width modulation-based high-frequency resonance suppression of high-speed railways," *IET Power Electron.*, vol. 8, no. 5, pp. 735–742, May 2015.

[4] H. Hu, H. Tao, F. Blaabjerg, X. Wang, Z. He, and S. Gao, "Train–network interactions and stability evaluation in high-speed railways—Part I: Phenomena and modeling," *IEEE Trans. Power Electron.*, vol. 33, no. 6, pp. 4627–4642, Jun. 2018.

[5] C. Hengbin, S. Wensheng, G. Xinglai, and F. Xiaoyun, "High-frequency resonance suppression of high-speed railways in China," *IET Elect. Syst. Transp.*, vol. 6, no. 2, pp. 88–95, Jun. 2016.

[6] J. Holtz and J. O. Krah, "Adaptive optimal pulse-width modulation for the line-side converter of electric locomotives," *IEEE Trans. Power Electron.*, vol. 7, no. 1, pp. 205–211, Jan. 1992.

[7] J. Holtz and H.-J. Kelin, "The propagation of harmonic currents generated by inverter-fed locomotives in the distributed overhead supply system," *IEEE Trans. Power Electron.*, vol. 4, no. 2, pp. 168–174, Apr. 1989.

[8] C. Heising, M. Oettmeier, V. Staudt, A. Steimel, and S. Danielsen, "Improvement of low-frequency railway power system stability using an advanced multivariable control concept," in *Proc. 35th Annu. Conf. IEEE Ind. Electron.*, Porto, Portugal, Nov. 2009, pp. 560–565.

[9] C. Heising, M. Oettmeier, R. Bartelt, V. Staudt, and A. Steimel, "Multivariable pole-placement control design for a single-phase 50-kW, 16.7-Hz railway traction line-side converter," in *Proc. Int. Conf. Power Eng., Energy Elect. Drives*, Lisbon, Portugal, Mar. 2009, pp. 273–278.

[10] Z. Shuai, H. Cheng, J. Xu, C. Shen, Y. Hong, and Y. Li, "A notch filter based active damping control method for low frequency oscillation suppression in train-network interaction systems," *IEEE J. Emerg. Sel. Topics Power Electron.*, to be published.
[11] X. Jiang, H. Hu, J. Yang, Y. Zhou, Z. He, Q. Qian, P. Tricoli, S. Hillmansen, and C. Roberts, "The mitigation technology of typical low-frequency voltage fluctuation in China electrified railway," in *Proc. Int. Symp. Power Electron., Elect. Drives, Automat. Motion*, Jun. 2018, pp. 632–637.
[12] X. Zhang, J. Chen, G. Zhang, L. Wang, R. Qiu, and Z. Liu, "An active oscillation compensation method to mitigate high-frequency harmonic instability and low-frequency oscillation in railway traction power supply system," *IEEE Access*, vol. 6, pp. 70359–70367, 2018.
[13] X. Zhang, L. Wang, W. Dunford, J. Chen, and Z. Liu, "Integrated full-frequency impedance modeling and stability analysis of the train-network power supply system for high-speed railways," *Energies*, vol. 11, no. 7, p. 1714, Jul. 2018.
[14] H. Tao, H. Hu, X. Zhu, Y. Zhou, and Z. He, "Harmonic instability analysis and suppression method based on $\alpha\beta$-frame impedance for trains and network interaction system," *IEEE Trans. Energy Convers.*, vol. 34, no. 2, pp. 1124–1134, Jun. 2019.
[15] H. Hu, H. Tao, X. Wang, F. Blaabjerg, Z. He, and S. Gao, "Train–network interactions and stability evaluation in high-speed railways —Part II: Influential factors and verifications," *IEEE Trans. Power Electron.*, vol. 33, no. 6, pp. 4643–4659, Jun. 2018.
[16] Y. Liao, Z. Liu, G. Zhang, and C. Xiang, "Vehicle-grid system modeling and stability analysis with forbidden region-based criterion," *IEEE Trans. Power Electron.*, vol. 32, no. 5, pp. 3499–3512, May 2017.
[17] H. Tao, H. Hu, X. Wang, F. Blaabjerg, and Z. He, "Impedance-based harmonic instability assessment in a multiple electric trains and traction network interaction system," *IEEE Trans. Ind. Appl.*, vol. 54, no. 5, pp. 5083–5096, Sep./Oct. 2018.
[18] Q. Lian, F. Lin, W. Shi, Z. Yang, H. Sun, J. Jiao, and Z. Zhang, "Analysis of nonlinear oscillation of four-quadrant converter in high-speed trains based on discrete model," in *Proc. 41st Annu. Conf. IEEE Ind. Electron. Soc. (IECON)*, Yokohama, Japan, Nov. 2015, pp. 002124–002129.
[19] X. Zhang, G. Zhang, L. Jiang, and Z. Liu, "The research on solution of voltage interruption of network-side converter in dual-power EMU," in *Proc. Int. Conf. Electr. Inf. Technol. Rail Transp.* Berlin, Germany: Springer, 2016, pp. 113–122.
[20] X. Wang, F. Blaabjerg, and M. Liserre, "An active damper to suppress multiple resonances with unknown frequencies," in *Proc. IEEE Appl. Power Electron. Conf. Expo. (APEC)*, Fort Worth, TX, USA, Mar. 2014, pp. 2184–2191.
[21] J. Holtz and J. O. Krah, "On-line identification of the resonance conditions in the overhead supply line of electric railways," *Arch. Elektrotechn.*, vol. 74, no. 1, pp. 99–106, May 1990.
[22] X. Zhang, J. Chen, G. Zhang, R. Qiu, and Z. Liu, "The WRHE-PWM strategy with minimized THD to suppress high-frequency resonance instability in railway traction power supply system," *IEEE Access*, vol. 7, pp. 104478–104488, 2019.

XINYU ZHANG was born in Jilin, China, in 1991. She received the B.S. degree from Beijing Jiaotong University, Beijing, China, in 2014, where she is currently pursuing the Ph.D. degree in electrical engineering.

She was a Visiting Student of electrical and computer engineering with The University of British Columbia, BC, Canada. Her research interests include modeling and control of high-speed trains, high power traction converters, stability analysis of train, and traction networks.

JIE CHEN was born in Zhejiang, China, in 1986. He received the B.S. degree and the Ph.D. degree in electrical engineering and automation from Beijing Jiaotong University, Beijing, China, in 2008 and 2013, respectively.

He was a Visiting Scholar of WEMPEC with the University of Madison. Since 2013, he has been a Postdoctoral Researcher with Beijing Jiaotong University and with the Institute of Electrical Engineering, Chinese Academy of Sciences, Beijing. His research interests include variable frequency drive, rail transportation traction control, and inverter parallel control.

RUICHANG QIU was born in Henan, China, in 1968. He received the B.S. degree in electrical engineering and automation, in 1993.

From 1990 to 2005, he was a Lecturer with the School of Electrical Engineering, Beijing Jiaotong University, where he is currently an Associate Professor. His current research interests include intelligent detection technology, power electronics and power conversion technology, electric traction, and transmission control.

ZHIGANG LIU was born in Shandong, China, in 1961. He received the bachelor's, master's, and Ph.D. degrees in electric drive for locomotives from Beijing Jiaotong University, Beijing, China, in 1986, 1990, and 1994, respectively.

In recent years, he presided over a number of national key scientific research projects and achieved fruitful results in the field of rail transit power supply, traction control, safety prediction and control, and so on. He is currently a Full Professor with Beijing Jiaotong University. He published a book on power electronics and spent several months as a Visiting Scholar in USA and Canada. His teaching activities and research interests include power electronics circuit and systems, rail transportation traction control and safety, and so on.

Dr. Liu is a Vice Chairman of the China Electro-technical Society Rail Transport Electrical Technical Committee, and he is also an evaluation expert of several national key plans.